Electro-osmotic Flow in Nanochannels with Voltage-Controlled Polyelectrolyte Brushes: Dependence on Grafting Density and Normal Electric Field

Qianqian Cao,[1] Chuncheng Zuo,[1] Lujuan Li,[1] Yinhe Zhang,[2] Guang Yan[1]

[1]College of Mechanical Science and Engineering, Jilin University, Changchun 130022, China

[2]Changchun Institute of Optics, Fine Mechanics and Physics, Chinese Academy of Sciences, Changchun 130033, China

Correspondence to: Q. Cao (E-mail: qqcao07@mails.jlu.edu.cn) or G. Yan (E-mail: yanguang07@mails.jlu.edu.cn)

Received 18 January 2012; revised 7 March 2012; accepted 14 March 2012; published online 2 April 2012
DOI: 10.1002/polb.23069

ABSTRACT: Molecular dynamics simulations were performed for electro-osmotic flow (EOF) confined in a polyelectrolyte-grafted nanochannel under variable grafting density and normal electric field. With decreasing the value of the normal electric field, the brush undergoes a collapse transition, and the ion distribution is changed significantly. The brush thickness increases on increasing the grafting density at positive and weak negative electric fields, whereas a reduced brush thickness is observed at strong negative electric field. Our results further reveal that the flow velocity is not only dependent on conformational transition of the brush but also related to the cation and anion distributions. At low grafting density, the EOF is almost completely quenched at high electric field strength due to strong surface friction between ions and walls. For the case of very dense grafting, the flow velocity is influenced weakly within the brush when varying the grafting density. Additionally, a bidirectional flow occurs at an intermediate electric field. The investigation on fluid flux indicates that the fluid flux is insensitive to the grafting density, when the normal electric field is removed. For nonzero normal electric fields, a significant change in the fluid flux is observed at low grafting densities. © 2012 Wiley Periodicals, Inc. J Polym Sci Part B: Polym Phys 50: 805–811, 2012

KEYWORDS: electro-osmotic flow; molecular dynamics; nanochannel; polyelectrolytes, nanotechnology, polyelectrolyte brush

INTRODUCTION The electro-osmotic flow (EOF) originates in the electrical double layer (EDL) at the solid–liquid interface and has been widely used as a pumping method in microfluidic and nanofluidic devices.[1,2] With the development and application of nanofluidics, nanochannels become key building blocks for the construction of lab-on-a-chip devices, which provide useful research tools for ion transport, bionanotechnology, investigation of single-molecular behavior, and biochemical analysis. More importantly, improving smart regulation of nanochannels has become a challenging topic for lab-on-a-chip development. Surface modification plays a critical role in implementing the functions of smart nanochannels. Recent studies have shown that polymers coated on the surface can control the EOF[3,4] and minimize wall–analyte interactions,[5,6] which is important for biomolecule separations using electrophoresis technology. In contrast to traditional electro-osmotic transport, the coupling between polymer chain dynamics and electrohydrodynamics creates a difficulty in predicting quantitatively the behavior of EOF in a polymer-bearing channel. There are a few studies that have paid attention to elucidate the modulation mechanisms of EOF in polymer-coated channels.[7–13] Theoretically, several important features on the controlling of EOF have been obtained by Harden et al.[7] at different grafting density regimes using a scaling approach, which can serve as a useful starting point to further study systems including the coupling of electrokinetic effects and polymer dynamics. Slater and coworkers[9,11] have performed coarse-gained molecular dynamics simulations of the EOF through a cylindrical nanopore coated with neutral polymers. Their findings confirm some of scaling predictions from Harden et al.[7] and are in good agreement with experimental observations.[14] Full atomistic molecular dynamics simulations have also been carried out by Qiao[8] to investigate the EOF confined between two opposing walls grafted with polymer layers, which provided a good understanding of the mechanisms of electro-osmotic transport modulated by neutral polymers. Recently, we have addressed the control mechanism of EOF inside a polymer-grafted nanochannel where polymers are exposed to a solvent of variable quality.[12,13] Our results showed that varying the solvent quality can affect significantly the flow velocity, counterion distribution, and conformational behavior of the polymer brush.

These works as mentioned above focused on investigations of the EOF through channels coated with neutral polymer

brushes. When polyelectrolyte chains are grafted densely to a solid surface, such as planar substrates and strongly curved surfaces of colloidal particles, a polyelectrolyte brush results.[15,16] The long-range electrostatic interaction in polyelectrolyte brushes brings about a variety of novel properties compared to polymer layers consisting of end-grafted neutral macromolecules. The polyelectrolyte brushes can respond to many external and internal stimuli, such as salt concentration, grafting density, pH, temperature, electric field, and charge fraction of the polyelectrolyte chain. A significant amount of works on the theory for polyelectrolyte brushes were carried out to understand their conformational characteristics, interactions, and phase behavior using scaling predictions[17–19] and self-consistent-field calculations.[20,21] Experimentally, chemists have designed and synthesized a number of novel polyelectrolyte brush systems with various specific functions that possess potential application value in colloid stability, flow regulation, smart surface, and membrane modification. For example, the integration of stimuli responsive polyelectrolyte brushes into solid-state single nanochannels can create tailor-made nanovalves resembling the functions of sophisticated biological ion channels.[22] The gating mechanism is implemented by collapse-stretching conformational transition of the brushes responsive to pH. Additionally, coating amphoteric molecules (lysine or histidine) onto the inner surface of an asymmetric nanometer-scaled channel permits a broad set of rectification properties and enables a higher degree of ion transport regulation.[23] More recently, Hou et al.[24] developed a pH gating ionic transport nanodevice using plasma asymmetric chemical modification with various complicated functional molecules coated onto the wall of single nanochannels to enhance the functionality of biological ion channels.

Obviously, the natural presence of charges in polyelectrolyte brush systems provides the possibility of using external electric fields to regulate their conformations. Moreover, the electric field represents a favorite approach to induce extension-collapse transition of polyelectrolyte brushes due to its faster construction than other stimuli. Ouyang et al.[25] used molecular dynamics simulations to analyze the gating mechanisms in a polyelectrolyte-grafted nanochannel under external electric field. Further, our group studied the effects of salt concentration and chain stiffness on response behavior of the brushes under added electric fields.[26] These works revealed that polyelectrolyte brushes as the gating components show a strong static and dynamic response to the change of applied electric field. Additionally, the experiment by Weir et al.[27] based on weak polybase brushes indicated that voltage-induced swelling exhibits a wider range of brush swelling states in comparison to pH switching. If such an electric field is incorporated into the transport of EOF in a polyelectrolyte-grafted channel, the coupling of polyelectrolyte chain dynamics and electrohydrodynamics may lead to some new electrokinetic transport phenomena. Compared to electro-osmosis transport in bare nanochannels without external electric fields normal to the wall, the formation and properties of the EDL will not only depend on the physicochemical properties of the surface but also on the electrostatic interactions of polyelectrolyte brushes with ions as well as the strength of normal electric fields. Recently, our group has performed molecular dynamics simulations of the electro-osmosis transport in a polyelectrolyte-grafted nanochannel under the control of a normal electric field.[28] In that work, we first addressed some problems on the interplay between complex EOF and nonequilibrium conformational behavior of polyelectrolyte brushes at a molecular level. We found that whether the channel surface is coated or not coated with polyelectrolytes leads to a very different flow behavior, and the fluid flux depends nonmonotonically on the normal electric field. This work based on our prior study[28] further takes into account the combination effects of grafting density and normal electric field on flow velocity, nonequilibrium brush thickness, fluid flux, and particle density distribution. We show how the direction and magnitude of normal electric field influence fluid transport and brush conformation at different grafting densities. The rest of the article is organized as follows. The details of the model system and molecular dynamics method are described in the next section. Then, we present simulation results and a detailed discussion of the results. Finally, we summarize our results in "Conclusions" section.

METHODOLOGY

System Model

We use the same parameters of the model as in our previous work,[28] such as molecular model of polyelectrolyte chains, wall parameters, fluid number density ($\rho_f = 0.8\sigma^{-3}$), number density of charged surface particles ($\rho_c = -0.1\sigma^{-2}$, the surface charges are negative), and salt concentration ($n_0 = 0.02\sigma^{-3}$). The polyelectrolyte chains with $N = 22$ monomers are grafted to the bottom wall, and the top wall is not bearing a brush as shown in Figure 1. The grafting points are arranged in a square lattice with a spacing $d = \rho_g^{-1/2}$, where ρ_g denotes the number of end-grafted chains per unit area. Every second monomer carries a negative charge. The cations in the bulk fluid include the counterions dissociated from polyelectrolytes and the dissociated salt cations. Our bead-spring model can be viewed as a coarse-grained representation of a flexible polyelectrolyte, for example, sodium poly(styrene sulfonate), which is an anionic polyelectrolyte and frequently chosen as the grafted polymer. The dimensions of the simulation box are $L_x \times L_y \times H$, where $L_x \times L_y \times 28.573\sigma$ and the height $H = 23\sigma$ along the z-direction (not including the wall thickness).

Molecular Dynamics Simulations

The short-range interaction between any two particles is modeled by a purely repulsive Lennard-Jones potential. We take σ, m, and ε_{LJ} as length, mass, and energy units, respectively. In this work, σ is also regarded as the particle diameter, chosen to be the same irrespective of the particle type. All other units are derived from these basic units, such as time unit $\tau = (m\sigma^2/\varepsilon_{LJ})^{1/2}$, temperature unit $T^* = \varepsilon_{LJ}/k_B$ (k_B is Boltzmann's constant), electric field unit $E^* = \varepsilon_{LJ}\sigma^{-1}/(4\pi\varepsilon LJ)^{1/2}$ (ε_0 is the vacuum permittivity), and velocity unit

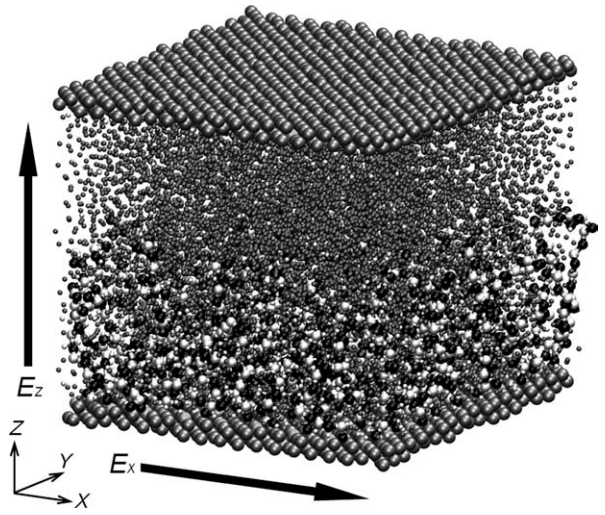

FIGURE 1 Snapshot of a simulation box containing movable particles (ions and solvent) through a polyelectrolyte-grafted channel with $\rho_g \approx 0.12\sigma^{-2}$. The EOF is generated by applying an electric field E_x along the x-axis, and an electric field E_z is applied normal to the wall to control the brush conformation. White and black beads linked by bonds represent charged and neutral monomers, respectively. Solvent particles and free ions are represented as small beads. The wall beads are made up of large gray beads.

$u^* = \sigma/\tau$. The chain's connectivity is maintained by a finitely extendable nonlinear elastic potential with bond stiffness $k_b = 30\varepsilon_{LJ}/\sigma^2$ and maximum bond length $R_0 = 1.5\sigma$. The choice of parameters corresponds to an average bond length of $l_b \approx 0.98\sigma$. Long-range electrostatic interactions are calculated using the particle-particle/particle-mesh (PPPM) algorithm.[29] In all simulations, the Bjerrum length $\lambda_B = e^2/(4\pi\varepsilon_0\varepsilon_r k_B T)$ (ε_r is the dielectric constant of the solvent) is fixed at $\lambda_B = 2\sigma$. λ_B is 0.71 nm for water at room temperature. To calculate the Coulomb interaction of the systems with a slab geometry, which are periodic in the x- and y-direction and have a finite length in the z-direction, an empty volume with the height of nL_z (L_z denotes the z-direction length of simulation box) is inserted along the z-direction. For all runs, $n = 3$ is taken. In addition, a correction term is also added to the modified PPPM method.[30] The system temperature is controlled by a dissipative particle dynamics thermostat[31,32] with the friction coefficient $\gamma = 1.5\tau^{-1}$ and the desired temperature $T = 1.2T^*$. Periodic boundary conditions are applied along x and y directions. We apply an electric field E_x parallel to the channel wall to induce the migration of charged particles and E_z perpendicular to the channel wall to control the extension rate of polyelectrolyte brushes (Fig. 1). In this work, the horizontal electric field E_x is fixed at $0.35E^*$. The electric field is exerted on any charged particle with charge q in the form of an additional external force $q(E_x\mathbf{n} + E_z\mathbf{m})$, where $\mathbf{n}$ and $\mathbf{m}$ denote x and z directional unit vectors. The positions and velocities of the particles are calculated using the velocity Verlet algorithm with a time step $\Delta t = 0.05\tau$. The system is equilibrated for 4.5×10^5 time steps, and then external electric fields are added through a further run of 5.5×10^5 time steps. After achieving a steady state, a production run from 2×10^6 to 2×10^7 time steps is performed to sample the simulation data depending on the strength of external electric field.

RESULTS AND DISCUSSION

Density Profiles and Brush Thickness

First, we investigate the conformational behavior of the brush under EOF shear with applied horizontal electric field $E_x/E^* = 0.35$ and different normal electric fields. Figure 2 shows monomer density profiles at a low grafting density $\rho_g = 0.031\sigma^{-2}$ and a high grafting density $\rho_g = 0.31\sigma^{-2}$. As seen from this figure, when E_z increases from $-3E^*$ and $3E^*$, the brush undergoes a collapse transition due to enhanced electric force toward the bottom wall. At $E_z/E^* = -3$, the density profile exhibits significant oscillation especially for $\rho_g = 0.031\sigma^{-2}$ [Fig. 2(a)]. Such strong oscillation reveals monomers that are in an ordered arrangement along the direction normal to the wall, corresponding to highly extended brush conformation. In this work, to calculate the average quantities, we divide the entire region into bins with thickness $L_b = 0.2\sigma$ (which is less than the average bond length $l_b \approx \sigma$) along the z direction (namely the direction normal to the wall). If a larger bin thickness is used, the

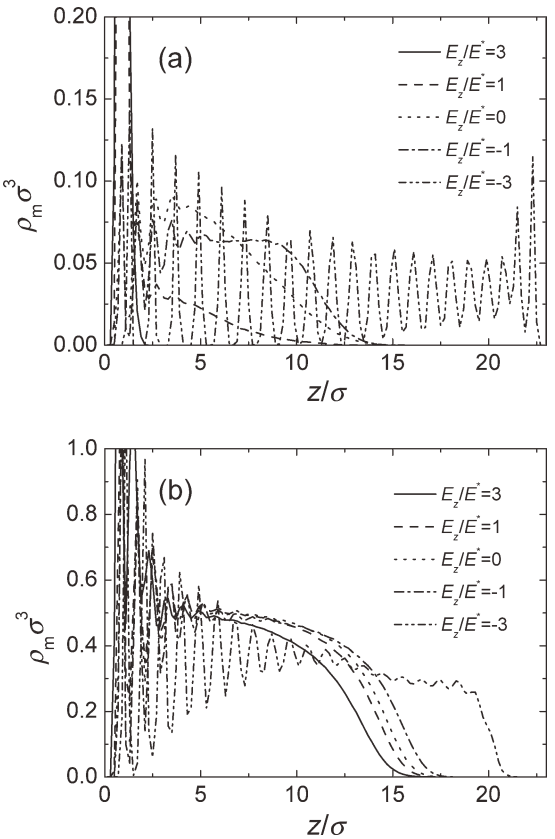

FIGURE 2 Monomer density profiles at (a) $\rho_g \approx 0.031\sigma^{-2}$ and (b) $0.31\sigma^{-2}$ for different normal electric fields. Simulations are performed at a constant parallel electric field $E_x/E^* = 0.35$.

oscillation behavior of monomer density may disappear under strong electric fields, just as observed in the work of Ouyang et al.[33] In their work, all polyelectrolyte chains under strong electric fields are in a highly extended state and monomer density profiles exhibit a flat shape except for the two ends of the brush. It is found that at $\rho_g = 0.031\sigma^{-2}$ the brush conformation is more sensitive to the change of normal electric field compared to the case of high grafting density $\rho_g = 0.31\sigma^{-2}$ [Fig. 2(b)]. At strongly positive electric field $E_z/E^* = 3$, a completely collapsed brush conformation can be observed at $\rho_g = 0.031\sigma^{-2}$ [Fig. 2(a)]. The brush at $\rho_g = 0.31\sigma^{-2}$ exhibits Gaussian-terminated parabolic shape when $E_z/E^* \geq -1$ [Fig. 2(b)].

The change of normal electric field not only affects the monomer density profiles but also has a large influence on the ion distribution. Figure 3 gives density profiles of anions and cations at $\rho_g = 0.031\sigma^{-2}$ for various normal electric fields E_z. At $E_z/E^* = 3$, anions [Fig. 3(a)] and cations [Fig. 3(b)] aggregate near bottom and top walls, respectively. With decreasing the value of electric field strength, more anions move toward the top wall, whereas more cations move toward the opposite wall. Strong electric fields can overcome the weaker electrostatic attraction between cations and charged monomers as well as the attraction between cations and anions. At $|E_z/E^*| = 3$, almost all cations are separated from the charged monomers or anions, and ions pack densely together near the walls. At $E_z/E^* = 0$ and 1, ions distribute along the direction normal to the wall and fill the entire channel. At high grafting density $\rho_g = 0.31\sigma^{-2}$ (Fig. 4), anion and cation densities show a different distribution compared to those at $\rho_g = 0.031\sigma^{-2}$. Clearly, most anions aggregate near the top wall at $E_z/E^* < -1$ [Fig. 4(a)]. However, only a small amount of anions distribute near the bottom wall, though a strong positive electric field $E_z/E^* = 3$ is applied. Note that at high grafting densities, a compact polyelectrolyte layer is formed near the bottom wall. Additionally, there exist strong repulsive interactions between the brush and anions. These factors make it difficult for most anions to penetrate into the brush and approach the bottom wall. Therefore, there are very few anions in a wide region away from the bottom wall.

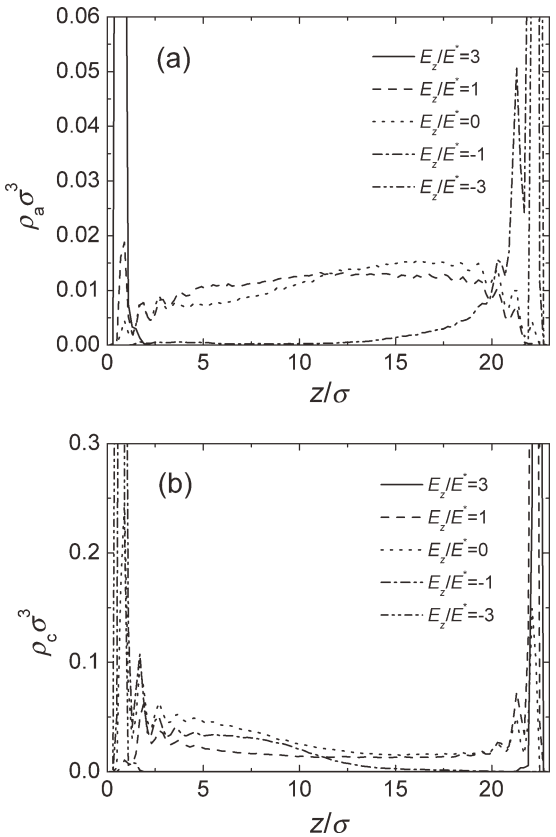

FIGURE 3 Density profiles of (a) anions and (b) cations at $\rho_g \approx 0.031\sigma^{-2}$ for different normal electric fields. The parallel electric field is fixed at $E_x/E^* = 0.35$.

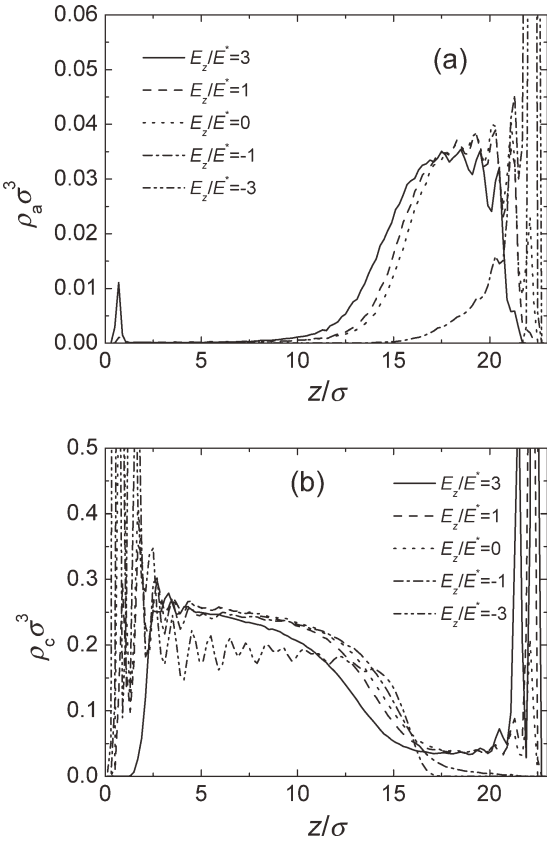

FIGURE 4 Density profiles of (a) anions and (b) cations at $\rho_g \approx 0.31\sigma^{-2}$ for different normal electric fields. The parallel electric field is fixed at $E_x/E^* = 0.35$.

To analyze quantitatively effects of grafting density and normal electric field on the extension or shrinkage of the brush, we calculate the average thickness of grafted layer using the formula $h = \langle[\sum_{i=1}^{Ng} z_i^{max}]/N_g\rangle$, where z_i^{max} is the maximum value of z-coordinates of the monomers from the ith polymer chain, and N_g denotes the number of grafted polyelectrolyte chains. Figure 5 shows the brush thickness h as a function of the grafting density at different normal electric fields. It is clear that the brush becomes thicker when decreasing

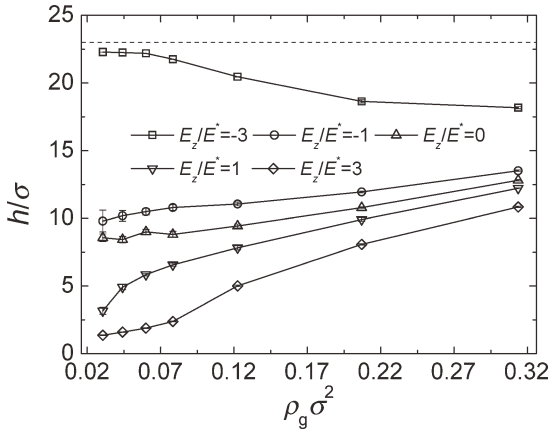

FIGURE 5 Average thickness h of polyelectrolyte brushes as a function of grafting density at different normal electric fields. The horizontal dashed line denotes the channel width. Simulation data are obtained at a fixed parallel electric field $E_x/E^* = 0.35$.

normal electric field from $E_z/E^* = 3$ to -3. At high grafting densities, the effect of electric field on the brush thickness becomes weak. In the absence of normal electric field, the brush thickness shows only a slight change at low grafting densities followed by a swelling of the brush, which is in consistence with previous works on equilibrium brush conformations (see Fig. 9 in ref. [34]). At relatively low grafting densities, the equilibrium structure of the polyelectrolyte brush is determined by a competition between electrostatic repulsion among the chains that tends to straighten them and a moderation of this effect by counterions that screen the interactions between polyelectrolyte monomers. Excluded volume effects start to become very dominant at high grafting densities. Here, we simply determine the critical grafting density ρ_g^* between the mushroom and brush regimes in the absence of E_z, namely through observing the change of the brush thickness (because the increase of the thickness with increasing the grafting density is a typical behavior for the brush conformations). We found that when $\rho_g > 0.078\sigma^{-2}$ the brush thickness shows a significant increase with the grafting density. Therefore, it is believed that the critical grafting density ρ_g^* is about $0.078\sigma^{-2}$. Certainly, the horizontal electric field E_x also plays an important role in controlling the brush structure due to shear force induced by particle motion driven by E_x, just as the case of EOF modulated by neutral brushes.[9,12] In this work, we fix E_x at a certain value, that is, the effect of E_x on flow characteristics is not discussed. When $E_z/E^* \geq -1$, the brush thickness increases as the grafting density is growing. Interestingly, increasing the grafting density leads to a reduced brush thickness at $E_z/E^* = -3$. The presence of applied normal electric fields leads to a rearrangement of positively and negatively charged ions as seen from Figures 3 and 4. At strong electric fields, a significant amount of anions and cations move toward two different surfaces. This nonequilibrium ion distribution further results in the formation of an internal electric field along the direction opposite to external electric field, which can resist stretching or shrinkage of grafted chains induced by the electric field. Note that at $E_z/E^* = -3$ the brush is in a fully extended state for low grafting densities. The increase of grafting density corresponds to an increase of charged particles per unit area further leading to the enhancement of the internal electric field.

Flow Velocity and Fluid Flux

In this section, the effects of grafting density and normal electric field strength on flow characteristics are addressed. We present the velocity profiles for different normal electric fields at $\rho_g = 0.031\sigma^{-2}$ and $0.031\sigma^{-2}$ in Figure 6. For bare nanochannel (namely the channel without grafted polyelectrolytes), a plug-like velocity profile can be observed in the absence of normal electric field.[9,28] At $E_z/E^* = 0$, the velocity profile at $\rho_g = 0.031\sigma^{-2}$ also shows a plug-like shape [Fig. 6(a)], while the shape of velocity profile is significantly changed at $\rho_g = 0.31\sigma^{-2}$ [Fig. 6(b)]. Additionally, a nonzero normal electric field applied can strongly affect the flow state in bare channels[28] and polyelectrolyte-grafted ones (Fig. 6). At $E_z/E^* = 1$, the flow velocity shows significant negative values near the top wall regardless of low or high grafting densities. This indicates that particles move along the direction of electric field, that is, more anions aggregate near the top wall as seen from Figures 3 and 4. However, in

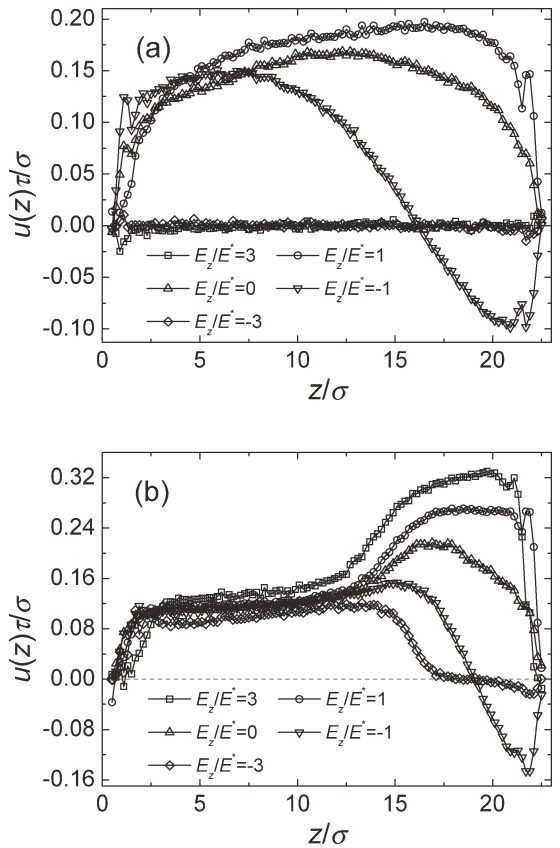

FIGURE 6 Steady-state flow velocity profiles at (a) $\rho_g \approx 0.031\sigma^{-2}$ and (b) $0.31\sigma^{-2}$ for different normal electric fields. Simulations are performed at a constant parallel electric field $E_x/E^* = 0.35$.

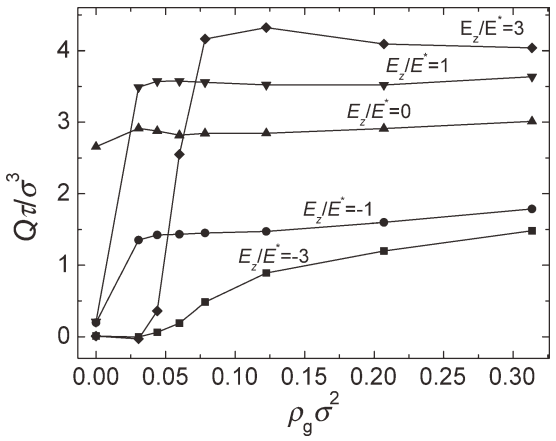

FIGURE 7 Fluid flux Q as a function of grafting density at different normal electric fields. Simulations are performed at a constant parallel electric field $E_x/E^* = 0.35$.

the case of sparse grafting ($\rho_g = 0.031\sigma^{-2}$), EOF is almost completely suppressed under strong electric fields $E_z/E^* = -3$ and 3 [Fig. 6(a)]. The similar phenomenon also occurs in bare channel.[28] Though cations and anions are completely pulled toward two different walls at strong electric fields, the bidirectional flow is not observed. It reveals that strong normal stress toward the walls induces strong surface friction between ions and walls with fcc microscopic structure, which further suppresses the movement of ions or EOF transport. Clearly, a strong flow occurs at weak electric fields. In a bare channel, the velocity profile exhibits a Couette-like shear flow induced by the migration of ions near the walls at intermediate electric fields, such as $E_z/E^* = 1$ and -1.[28] Such flow feature is not observed in the case of sparsely grafted-polymers [Fig. 6(a)]. This can be attributed to the friction drag of polyelectrolyte brush and the presence of polyelectrolyte counterions (though for sparsely grafted-polymer channel).

At high grafting density $\rho_g = 0.31\sigma^{-2}$, the flow velocity within polyelectrolyte brush is insensitive to the change of electric field [Fig. 6(b)]. Outside the brush varying the electric field can cause an obvious change in the flow velocity. It is found that a significant amount of cations are located in the brush [Fig. 4(b)], and only a small part of anions are collected near the bottom wall at $E_z/E^* = 3$ [Fig. 4(a)]. Therefore, particles driven by cations move along the direction of horizontal electric field E_x in a wide region away from the polyelectrolyte-grafted wall. Note that the flow velocity in the brush approximately remains constant. Additionally, though most cations distribute in the brush, the particles move with a relatively slow velocity. This is due to that the dense grafting creates much stronger resistance to particle flow in the brush. At $E_z/E^* = -3$, the brush adopts a strongly extended conformation, and its free end nearly reaches the top wall. The EOF in the region of $z > 17\sigma$ is almost completely quenched, while a significant flow flux occurs near the bottom wall. It reveals that the flow velocity is related not only to brush stretching/shrinking conformations but also to ionic distribution. From cation density profiles, the cation density is close to zero in the region of $z > 17\sigma$, and anions aggregate near the top wall. Therefore, strong friction between anions and the top wall and extended brush conformation (cations are confined within the brush) result in a quenched flow near the top wall.

As discussed before, the flow velocity shows a strong dependence on the grafting density and normal electric field, and some complex flow phenomena are observed under the influence of these factors. Here, we calculate the fluid flux $Q = \int_0^{Ly}\int_0^H u(z)dzdy$ as a function of grafting density for different electric fields in Figure 7. From the figure, we find that there is a different response behavior of the flux to the change of electric field at different grafting densities. For the case without normal electric field, there is a slight difference of the flux in the presence or absence of polyelectrolyte grafting. Clearly, increasing the grafting density leads to a decrease of the effective width of the channel. Therefore, this will reduce the flux for neutral polymer coating, which is in agreement with the results obtained in our previous works on the control of EOF by neutral polymer brush.[12] Furthermore, the friction interaction within the brush is also enhanced, as the brush becomes denser. However, for the case of the polyelectrolyte brush, the increase of the grafting density also corresponds to the increase of counterions, which can compensate the reduction of the flux caused by the reduced channel width and enhanced friction. As a result, the EOF under the control of the polyelectrolyte brush shows a weak dependence on the grafting density under the absence of a normal electric field. Under added nonzero electric fields, the flux shows an obvious change at low grafting densities. For bare channel and channel with sparsely grafted polyelectrolytes, strong electric fields can suppress the flow even at strong positive electric fields. Further increasing the grafting density does not cause a significant change of the flux. For channels grafted with neutral polymers, the EOF is strongly quenched by the polymer coating at high grafting densities.[9] At strong negative electric field $E_z/E^* = -3$, the flux has a monotonic dependence on the grafting density. When the direction of electric field is reversed, the flux shows a maximum at an intermediate grafting density $\rho_g \approx 0.12\sigma^{-2}$. Clearly, at high grafting densities, when the electric field increases from $E_z/E^* = -3$ to 3, the flux also exhibits a gradually increasing tendency.

CONCLUSIONS

We have performed molecular dynamics simulations to investigate EOF confined in a polyelectrolyte-grafted nanochannel. The combination effects of normal electric field E_x and grafting density ρ_g on conformational behavior of polyelectrolyte brushes, ion distribution, and flow characteristics are addressed. From monomer density profiles, we find that the brush conformation at high grafting density exhibits a relatively weak response to normal electric field compared to low grafting density. It is believed that at high grafting density, a stronger internal electric field along the direction opposite to normal electric field as well as enhanced

excluded volume interactions within the brush can resist stretching or shrinkage of grafted chains. Our studies reveal that the properties of EOF are significantly changed under the influence of normal electric field. Clearly, varying normal electric field can control the extension or shrinkage of the brush and further affect the effective width of the channel to implement the modulation of fluid flux. However, the fluid flux does not depend monotonously on normal electric field, that is, the flow characteristics are not related to the conformational transition of the brush. For the case of pressure-driven flow in a nanofluidic channel grafted with polyelectrolytes, the fluid flux is monotonously dependent on the normal electric field.[25] It is demonstrated that the change of ion density along the direction normal to the wall induced by normal electric field plays a critical role in modulating the EOF. Under strong normal electric fields, the EOF is almost completely quenched at low grafting density due to high surface friction between ions and walls. Unlike the case of low grafting density, significant changes in the flow velocity occur outside the brush or near the wall without grafting at high grafting density. Although increasing the grafting density leads to the increase of cation density (which can enhance the EOF), the friction effects in the brush also become stronger. This work also shows that the dependence of fluid flux on the grafting density is affected to a considerable degree by normal electric field.

ACKNOWLEDGMENTS

This work was supported by the National Natural Science Foundation of China (Nos. 30770501 and 51175223).

REFERENCES AND NOTES

1 Stone, H. A.; Stroock, A. D.; Ajdari, A. *Annu. Rev. Fluid Mech.* **2004,** *36*, 381–411.

2 Squires, T. M.; Quake, S. R. *Rev. Mod. Phys.* **2005,** *77*, 977–1026.

3 Paumier, G.; Sudor, J.; Gue, A. M.; Vinet, F.; Li, M.; Chabal, Y. J.; Esteve, A.; Djafari-Rouhani, M. *Electrophoresis* **2008,** *29*, 1245–1252.

4 Ma, D.; Chen, H. W.; Shi, D. Y.; Li, Z. M.; Wang, J. F. *J. Colloid Interface Sci.* **2009,** *332*, 85–90.

5 Haselberg, R.; van der Sneppen, L.; Ariese, F.; Ubachs, W.; Gooijer, C.; de Jong, G. J.; Somsen, G. W. *Anal. Chem.* **2009,** *81*, 10172–10178.

6 Feng, J. J.; Wang, A. J.; Fan, J.; Xu, J. J.; Chen, H. Y. *Anal. Chim. Acta* **2010,** *658*, 75–80.

7 Harden, J. L.; Long, D.; Ajdari, A. *Langmuir* **2001,** *17*, 705–715.

8 Qiao, R. *Langmuir* **2006,** *22*, 7096–7100.

9 Tessier, F.; Slater, G. W. *Macromolecules* **2006,** *39*, 1250–1260.

10 Qiao, R.; He, P. *Langmuir* **2007,** *23*, 5810–5816.

11 Hickey, O. A.; Harden, J. L.; Slater, G. W. *Phys. Rev. Lett.* **2009,** *102*, 108304.

12 Cao, Q. Q.; Zuo, C. C.; Li, L. J.; Ma, Y. H.; Li, N. *Microfluid. Nanofluid.* **2010,** *9*, 1051–1062.

13 Cao, Q. Q.; Zuo, C. C.; Li, L. J.; Yang, Y.; Li, N. *Microfluid. Nanofluid.* **2011,** *10*, 977–990.

14 Doherty, E. A. S.; Berglund, K. D.; Buchholz, B. A.; Kourkine, I. V.; Przybycien, T. M.; Tilton, R. D.; Barron, A. E. *Electrophoresis* **2002,** *23*, 2766–2776.

15 Rühe, J.; Ballauff, M.; Biesalski, M.; Dziezok, P.; Grohn, F.; Johannsmann, D.; Houbenov, N.; Hugenberg, N.; Konradi, R.; Minko, S.; Motornov, M.; Netz, R. R.; Schmidt, M.; Seidel, C.; Stamm, M.; Stephan, T.; Usov, D.; Zhang, H. N. *Adv. Polym. Sci.* **2004,** *165*, 79–150.

16 Ballauff, M. *Prog. Polym. Sci.* **2007,** *32*, 1135–1151.

17 Zhulina, E. B.; Borisov, O. V.; Birshtein, T. M. *Macromolecules* **1999,** *32*, 8189–8196.

18 Csajka, F. S.; Netz, R. R.; Seidel, C.; Joanny, J. F. *Eur. Phys. J. E* **2001,** *4*, 505–513.

19 Pincus, P. *Macromolecules* **1991,** *24*, 2912–2919.

20 Zhulina, E. B.; Wolterink, J. K.; Borisov, O. V. *Macromolecules* **2000,** *33*, 4945–4953.

21 Borisov, O. V.; Leermakers, F. A. M.; Fleer, G. J.; Zhulina, E. B. *J. Chem. Phys.* **2001,** *114*, 7700–7712.

22 Yameen, B.; Ali, M.; Neumann, R.; Ensinger, W.; Knoll, W.; Azzaroni, O. *Nano Lett.* **2009,** *9*, 2788–2793.

23 Ali, M.; Ramirez, P.; Mafe, S.; Neumann, R.; Ensinger, W. *ACS Nano* **2009,** *3*, 603–608.

24 Hou, X.; Liu, Y. J.; Dong, H.; Yang, F.; Li, L.; Jiang, L. *Adv. Mater.* **2010,** *22*, 2440–2443.

25 Ouyang, H.; Xia, Z. H.; Zhe, J. *Microfluid. Nanofluid.* **2010,** *9*, 915–922.

26 Cao, Q. Q.; Zuo, C. C.; Li, L. J.; Yan, G. *Biomicrofluidics* **2011,** *5*, 044119.

27 Weir, M. P.; Heriot, S. Y.; Martin, S. J.; Parnell, A. J.; Holt, S. A.; Webster, J. R. P.; Jones, R. A. L. *Langmuir* **2011,** *27*, 11000–11007.

28 Cao, Q. Q.; Zuo, C. C.; Li, L. J.; Zhang, Y. H. *Microfluid. Nanofluid.* **2012,** *12*, 649–655.

29 Hockney, R. W.; Eastwood, J. W. Computer Simulation Using Particles; Adam Hilger: Bristol, **1988.**

30 Yeh, I. C.; Berkowitz, M. L. *J. Chem. Phys.* **1999,** *111*, 3155–3162.

31 Hoogerbrugge, P. J.; Koelman, J. M. V. A. *Europhys. Lett.* **1992,** *19*, 155–160.

32 Español, P.; Warren, P. *Europhys. Lett.* **1995,** *30*, 191–196.

33 Ouyang, H.; Xia, Z. H.; Zhe, J. *Nanotechnology* **2009,** *20*, 195703.

34 Cao, Q. Q.; Zuo, C. C.; Li, L. *J. Eur. Phys. J. E* **2010,** *32*, 1–12.